Hindawi Publishing Corporation
Journal of Electrical and Computer Engineering
Volume 2012, Article ID 849638, 11 pages
doi:10.1155/2012/849638

Research Article

UWB Localization System for Indoor Applications: Concept, Realization and Analysis

Lukasz Zwirello, Tom Schipper, Marlene Harter, and Thomas Zwick

Institut für Hochfrequenztechnik und Elektronik, Karlsruhe Institute of Technology (KIT), Kaiserstraße 12, 76131 Karlsruhe, Germany

Correspondence should be addressed to Lukasz Zwirello, lukasz.zwirello@kit.edu

Received 29 October 2011; Accepted 4 February 2012

Academic Editor: Baoyong Chi

A complete impulse-based ultrawideband localization demonstrator for indoor applications is presented. The positioning method, along with the method of positioning error predicting, based on scenario geometry, is described. The hardware setup, including UWB transceiver and time measurement module, as well as the working principles is explained. The system simulation, used as a benchmark for the quality assessment of the performed measurements, is presented. Finally, the measurement results are discussed. The precise analysis of potential error sources in the system is conducted, based on both simulations and measurement. Furthermore, the methods, how to improve the average accuracy of 9 cm by including the influences of antennas and signal-detection threshold level, are made. The localization accuracy, resulting from those corrections, is 2.5 cm.

1. Introduction

In the recent decade, a growing interest in precise indoor locating systems could be observed. At the moment, several methods, based on different technologies, targeted for various environments are being investigated worldwide. They can be divided into acoustic [1, 2], optical [3], and radio frequency methods. The last type of methods can be divided into continuous wave (CW), for example, WLAN or RFID [4], and impulse signals. CW systems suffer however either from low accuracy, lack of immunity against multipath effects, or from requirement for large number of sensors. The short ultrawideband (UWB) pulses are ideal candidates for indoor localization applications. Their short duration assures the resistance against multipath effects and gives a supreme time resolution. Because of the fact that the UWB has a very strict power emission limits [5, 6], the short-range (e.g., indoor) applications are aimed for.

In this work, a complete process of designing a UWB positioning system is presented, starting from the choice of positioning method, through placement of access points, analysis of error sources in the UWB transceiver, and ending with simulation and measurement verification. The transmitter and receiver architecture, as well as the hardware used during the localization experiments, are briefly described, and for more details, respective references are placed in the paper.

This paper is structured as follows: first, the positioning method is described in Section 2, and the best algorithm, in terms of accuracy and computational effort, for solving the TDoA equations is determined. In Section 3, the consideration of optimal placement of receivers is given. Based on this, the positioning accuracy limit is derived. Section 4 is dedicated to the description of the constructed UWB transceiver and used for measurement validation, as well as to the TDoA measurement setup. In access to this, the influence of the used antenna type on localization precision and signal digitizing units will be described in Section 5; the correction algorithms for compensation of those two effects will be proposed here as well. In Section 6, a model of the laboratory room is presented, which was used for determination of the system capabilities. In the same section, also the simulation-based result quality prediction method, along with the localization results, is presented. The last Section 7 summarizes the presented work, followed by the conclusions and finally improvement proposals for future implementations.

2. Positioning Method

In order to choose the best suited positioning method for a specific application, first the boundary conditions have to be known. The aimed application scenario for the UWB system is the localization of mobile users (MUs) in indoor scenarios like, for example, office rooms or industrial halls. In such scenarios, the only prerequisite would be the access points (APs) which are aware of their own position.

Depending on the kind of positioning method, a synchronization between APs and MUs may be required or not. In the given scope of applications, where no information about the MU is given, only the relative time methods such as the time difference of arrival (TDoA) or the angle of arrival (AoA) method are suitable.

The TDoA method requires information about the signal propagation time from the MU (transmitter) to all the APs (receivers). For a 3D positioning, there are at least four APs needed. The resulting set of nonlinear equations can be solved either by iterative or direct methods (more on this in Section 2.2). In the AoA approach, an antenna array is used in each AP. Behind each array element, a UWB receiver is placed, and the difference in receive times is measured. Based on this, the angle of arrival for a signal can be determined by a linear equation. In this method in every AP, an antenna array consisting of at least three elements, aligned not in line, is required for 3D localization, and a minimum of two APs need to be used.

In the experiment presented in this paper, the TDoA method was utilized. It future application, it is advisable to combine the TDoA and AoA to achieve synergy effects [7].

There are two ways of performing the TDoA measurement in a system consisting of multiple APs and MUs:

(1) either the MU sends its user-specific information sequence, coded by UWB pulses, and it will be localized by a central processing unit (CPU), where the CPU synchronizes all the APs and collects the time measurement data,

(2) or the APs will be used only as repeaters. In this case, the MU receives back the transmitted signal, in addition containing the information from which AP (coordinates) it came. In this concept the MU has to calculate its own location, based on relative distance information to the reference nodes (APs) [8, 9]. This is based on the *two-way-ranging* measurement principle.

In this work, the first of the two presented alternatives was chosen. The second method would be more practical for the end application, especially in larger scenarios, due to the highly reduced wiring effort. In the general case, the positioning accuracy is only dependent on the time measurement precision, what will be shown in Section 3.

In the TDoA system, the time difference must be calculated in relation to a certain base receiver (BR), assigned index "1" in this work for convenience. The positions of the APs $\vec{r}_{Rj} = [x_{Rj}, y_{Rj}, z_{Rj}]$ are given, and the position of the MU $\vec{r}_T = [x_T, y_T, z_T]$ is unknown. The range difference equation between BR ($R1$) and transmitter (T) and any other receiver (R_j) has the following form:

$$c \cdot \Delta t_{1j} = \Delta d_{1j} = \left\|\vec{r}_T - \vec{r}_{R1}\right\| - \left\|\vec{r}_T - \vec{r}_{Rj}\right\|, \quad (1)$$

where the $j = 2, \ldots, N$ and N is the total number of APs. As a consequence of this, $N - 1$ linearly independent TDoA equations can be written and combined in a vector matrix

$$\vec{\rho} = [\rho_{12} \ldots \ \rho_{1N}]^T = [\Delta d_{12} \ldots \ \Delta d_{1N}]^T. \quad (2)$$

Like this, the $\vec{\rho}$ is the square root function of the distance differences. The solution can be found by linearizing this function around a starting point $\vec{r}_{T,0}$. The method of choosing the starting point will be described in Section 2.2. After moving the constant terms of the linearized equation to the left side, the following is achieved:

$$\Delta\vec{\rho} = H\Delta\vec{r}. \quad (3)$$

The $\Delta\vec{\rho}$ is the vector of residues, $\Delta\vec{r}$ is the solution vector, and H is the mapping matrix, relating the measured time differences to the differences between starting and calculated position. The least squares solution is in this case

$$\Delta\vec{r} = \left(H^T H\right)^{-1} H^T \Delta\vec{\rho}. \quad (4)$$

This iterative method can be continued by using the calculated position as another starting point

$$\vec{r}_T = \vec{r}_{T,0} + \Delta\vec{r} \quad (5)$$

and reperforming this until a breakup criterion is met. This algorithm can only work properly if the equations are not correlated with each other. For a real measurement however, this criterion is not satisfied.

2.1. Problem of the Correlation between Measurements. The reason for the correlation of the TDoA equations is the noise (e.g., thermal noise, receiver noise, and digitization noise). As a result of noise influence, (1) changes to

$$\Delta\widetilde{\rho}_{1,i} = \Delta\widetilde{d}_{1,i} = \left(\left\|\vec{r}_T - \vec{r}_{R1}\right\| + w_1\right) - \left(\left\|\vec{r}_T - \vec{r}_{Rj}\right\| + w_j\right), \quad (6)$$

where w_j denotes noise therm on the jth AP. From this, it is obvious that the measurement noise from the BR is present in all other measurements. This is independent of which receiver is chosen as a reference. Due to this, before calculating the positioning solution, the decorrelation has to be performed first. The measure of the correlation between all the elements of vector $\widetilde{\rho}$ is its covariance matrix. In a system where all receivers have the same architecture and consist of identical components and the time measurements are performed by the same hardware, the equal noise standard deviation σ_t for all APs can be safely assumed. Under this condition, the covariance matrix is fully occupied

$$R_{\Delta t} = \begin{pmatrix} 2\sigma_t^2 & \sigma_t^2 & \ldots & \sigma_t^2 \\ \sigma_t^2 & 2\sigma_t^2 & \ldots & \sigma_t^2 \\ \vdots & \vdots & \ddots & \vdots \\ \sigma_t^2 & \sigma_t^2 & \ldots & 2\sigma_t^2 \end{pmatrix}. \quad (7)$$

Should this fact be ignored, then for the same measurement a different positioning solution will be obtained every time the BR is changed. The decorrelation, also used in [10], can be done with the Cholesky decomposition of the covariance matrix

$$R_{\Delta t} = LDL^T. \tag{8}$$

The decorrelated matrix D results from the linear combination with L^{-1},

$$D = L^{-1} R_{\Delta t} L^{-1,T}, \tag{9}$$

and the measurement vector $\tilde{\vec{\rho}}$ has to be transformed with the matrix L^{-1} as well,

$$\tilde{\vec{\rho}}' = L^{-1}\tilde{\vec{\rho}}. \tag{10}$$

At this point, the decorrelated equation set can be linearized around a starting point, and the new measurement and mapping matrix have the form

$$\vec{\rho}' = L^{-1} \cdot \vec{\rho}, \tag{11}$$

$$H' = L^{-1} \cdot H. \tag{12}$$

The solution of (12) with the weighted least squares has the following form:

$$\Delta\vec{r} = \left(H'^T D^{-1} H'\right)^{-1} H'^T D^{-1} \cdot \Delta\vec{\rho} \tag{13}$$

and can be iteratively improved by applying (5). In this section, the method of decorrelating the TDoA measurements was presented with the subsequent solution with the Gauss-Newton algorithm. In the following one, the most efficient algorithm will be chosen.

2.2. Choice of the Best Suited Algorithm. To calculate the MU position from the measurement data, the error function (3) needs to be minimized. It is however not possible to investigate the value of this function for every input argument. Because of this, a number of dedicated algorithms for solving such a nonlinear problems were created. They all follow the same idea: first, a rough estimation of the solution is done, which then can be interpreted as a start point in the error landscape. From this point, a descent direction in the error landscape is calculated. The descent direction is calculated in a way that the reduction of the error function value is highly probable. Subsequently, a first step with a certain step width, from the starting point in the descent direction, is done. A new point is reached and serves as a new starting point to apply the same procedure again, until a stop criterion is met. This can be either the change in the error function or the change in the calculated position. If this value is small enough to assume the stationary condition, a global or local minimum is reached.

In this work, the following algorithms were implemented: Gauss-Newton (GN) with the *quadcubic*-line-search-procedure (qLSP), Levenberg-Marquardt (LM), trust-region-reflective algorithm (TRR), and the interior point (IP). The modified Bancroft algorithm (BA) was used as described in [11]. Those algorithms shall now be compared against each other, to state which is the best for the final system. The criteria are the following:

(i) the mean computation time, calculated as the average of computation times for a set of positions,

(ii) the accuracy of the solution, where the quality factor is the average 3D positioning error, calculated according to

$$\text{mean 3D error} = \frac{1}{M}\sum_{k=1}^{M}\left\|\vec{r}_{T_k} - \hat{\vec{r}}_{T_k}\right\|. \tag{14}$$

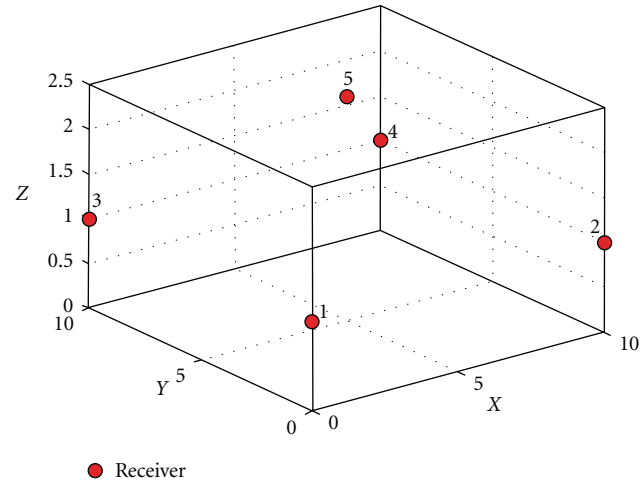

Figure 1: Scenario used for evaluation of localization algorithms.

Because of the fact that some of the evaluated algorithms do not have any additional constrains (e.g., volume in which the feasible solution should remain), large positioning errors can occur. This would largely afflict the average value. For this reason, in addition, the median value will be given.

For the evaluation, an imaginary room with dimensions 10 m/10 m/2.5 m with five APs was used. Four of the receivers were placed in 1 m height in the corners; the fifth one was placed in the middle point of the ceiling. This constellation is depicted in Figure 1. The reason for this AP distribution is explained in Section 3.

The TDoA data for the evaluation was obtained from (6). The measurement noise was modeled as normally distributed, with standard deviation $\sigma_t = 333$ ps (corresponding to $\sigma_d = 10$ cm). The assumption about homoscedasticity of the time error on every AP is made only for the sake of algorithm testing and does not apply during measurements. The MU positions were picked within the scenario boundaries, by a random function with equal distribution. The starting point for the iterative algorithms was chosen by the Bancroft algorithm, to see to which extent the positioning solution improvements are possible. The $M = 1000$ positions calculations were performed. The results are presented in Table 1. As a constraint for the interior-point and Bancroft

Table 1: Average 3D error and comutation times of various algorithms.

Algorithm	Average computation time [ms]	3D positioning error mean/ median [m]
Bancroft	0.580	0.406/0.312
Gauss-Newton	31.85	0.386/0.276
Levenberg-Marquardt	15.41	0.386/0.276
Trust region reflective	40.96	0.386/0.276
Interior point	98.10	0.311/0.251

algorithms, it was implied that the solution has to be within the room.

The first impression is that the GN delivers good results; however, if the starting point would be picked in random manner and not by BA, the convergence problems occur. From the other algorithms that are left, the BA has the shortest computation time, and its accuracy is smaller than in case of iterative algorithms. The LM and TRR are both in the similar accuracy range; however, the LM requires less computation time. The IP delivers the most precise results; however, this advantage is achieved on cost of the longest computation time from all of the evaluated algorithms.

Based on this result, the best combination seems to be the starting point determination based on the BA and adjacent final calculation with LM. A similar conclusion was drawn in [12]. In case where the additional conditions regarding the geometry should be accounted for, the IP is a good choice.

3. Optimal Access Point Distribution and Accuracy Prediction

If a real system should be deployed, at some point the question about optimal AP placement has to be answered. In order to solve this issue, the question shall be rephrased: "*How does an error in a time difference measurement maps to the positioning solution?*" The covariance matrix of the measurement vector $\vec{\rho}$ is defined by

$$R_\rho = H \cdot R_r \cdot H^T \tag{15}$$

and is related to the covariance matrix R_r of the positioning solution $\vec{r_T}$. H is the linearized mapping matrix from (3). When this is solved for R_r,

$$R_r = \left(H^T H\right)^{-1} H^T \cdot R_\rho \cdot H\left(H^T H\right)^{-1}, \tag{16}$$

the general expression for mapping of the measurement uncertainty on the localization uncertainty is obtained [13]. In case the signal propagation time measurements have the same variance σ_d^2, the covariance matrix of the measurement has the form of $R_\rho = \sigma_d^2 \cdot I$ and (16) reduces to

$$R_r = \left(H^T H\right)^{-1} \cdot \sigma_d^2,. \tag{17}$$

This is however only valid for uncorrelated measurements. This can be corrected by employing the decorrelated matrix H' from (12) [14]. The valid form for calculating the localization solution covariance matrix in the TDoA case has the following form:

$$R_r = \left(H'^T D^{-1} H'\right)^{-1} \cdot \sigma_d^2, \tag{18}$$

where the $\left(H'^T D^{-1} H'\right)^{-1} = Q$ and Q is due to the performed decorrelation a diagonal matrix. The entries of the diagonal give the DOP values in x-, y-, and z-direction. Those are called XDOP, YDOP, and VDOP (vertical dop). It is also possible to calculate the DOP values for 2D and 3D positions:

$$\begin{aligned} \text{HDOP} &= \sqrt{\sigma_x^2 + \sigma_y^2} = \sqrt{Q_{11} + Q_{22}}, \\ \text{VDOP} &= \sqrt{\sigma_z^2} = \sqrt{Q_{33}}. \end{aligned} \tag{19}$$

The mutual dependence of those values is given by PDOP:

$$\text{PDOP} = \sqrt{\text{HDOP}^2 + \text{VDOP}^2}. \tag{20}$$

Additional information on PDOP can be found [15].

Like this, PDOP, being a function only of T-R coordinates, can be used as a quality measure of a conceptualized T-R constellation. In general, high DOP values indicate poor and small DOPs good T-R configuration. A following example is prepared to gain a better impression of the meaning of this fact. In Figure 2, the distribution of HDOP and VDOP values in a 20 m/20 m/6 m-sized area, for three different constellations of access points, are presented.

Configuration 1 shows 5 receivers placed in 4 m height. HDOP inside of the constellation is in the range of $[1.1, \ldots, 3]$ and increases up to 9 outside of it. Concurrently, the VDOP stays in the range of $[2.2, \ldots, 6]$.

The VDOPs can be improved by shifting the middle station out of the plane of all other receivers, for example, 1 m upwards. This situation is depicted in *configuration 2*. The VDOP became better $[2.2, \ldots, 3.5]$, whereby HDOP did not undergo any significant change.

Another measure for improving the resolution in vertical direction is to involve additional station placed underneath all present receivers. This causes larger measured time differences between two neighbored transmitter positions. This is represented by *configuration 3*. Henceforth, the VDOP is in the range $[1.5, \ldots, 2.3]$. It is worth noticing that in all cases the system horizontal accuracy decreases rapidly as soon as the transmitter is outside the receiver constellation. In theory, almost infinite number of different configurations could be tested; however, when considering the practical aspects of base station placement in an average indoor scenario, additional constrains apply. As so, the lineups like in *configuration 3* from Figure 2 should be avoided. Although here the distribution of DOP values is most homogeneous, any station placed on the ground, or slightly above it, will be most likely not visible for MU due to shading effects caused by inside facilities. Because of the mentioned reasons, a similar distribution to this presented in *configuration 2* will be considered further. For practical reasons, during the measurements, a minor modification was undertaken, where the center top AP was shifted slightly to the side.

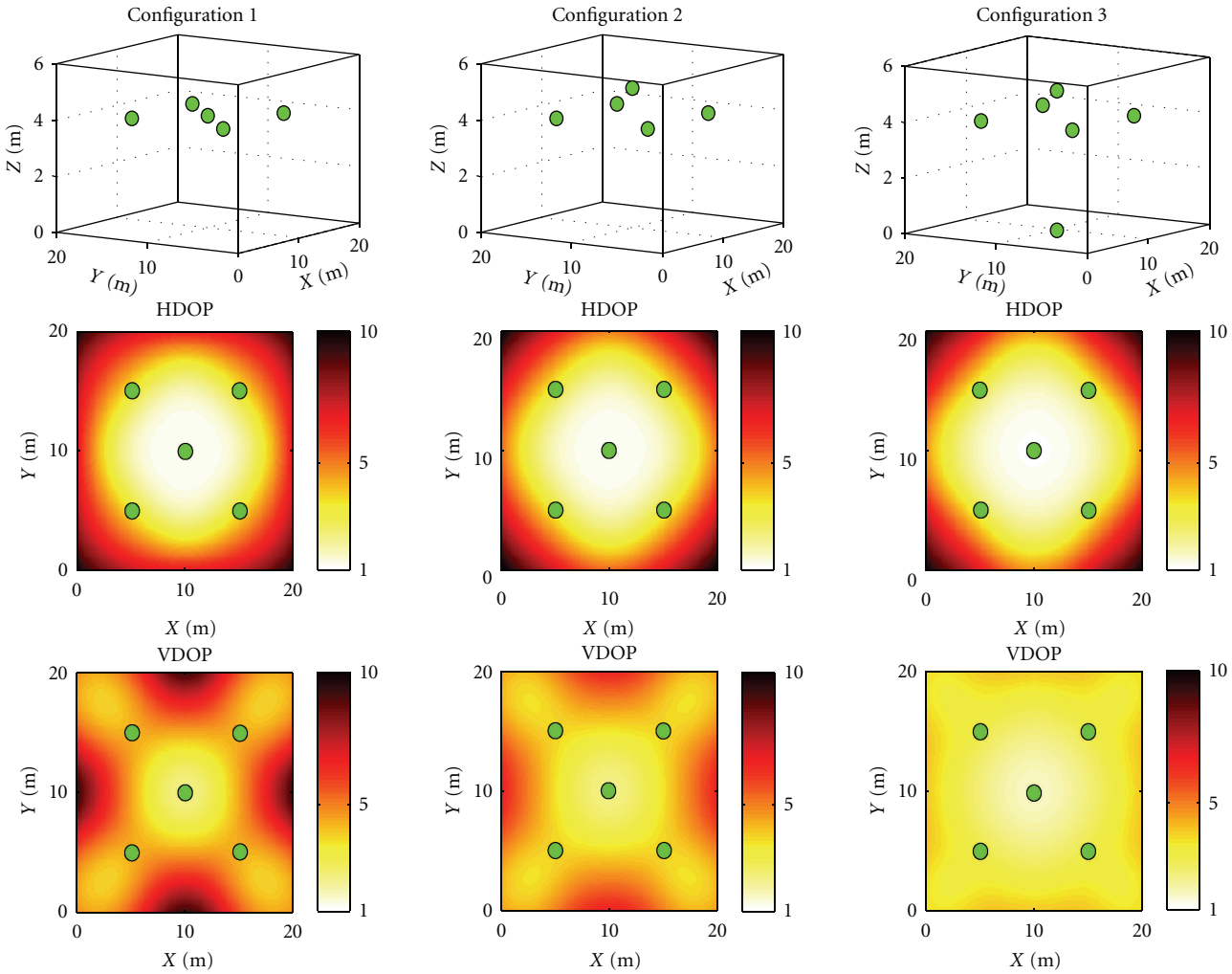

Figure 2: Spatial distribution of HDOP and VDOP values for three different access point configurations. The AP positions are marked with green dots.

It has to be mentioned that larger number of base stations would give a rise to more uniform distribution of DOPs and better performance in terms of shadowing; however, the cost of practical implementation would increase.

The very useful information that can be obtained from (20) is the influence of the TDoA measurement error on the localization solution. By knowing the standard deviation of time measurement (σ_{time}) and a PDOP value, the positioning accuracy can be predicted

$$\sigma_{\text{pos3D}} = \sigma_d \cdot \text{PDOP}, \tag{21}$$

where $\sigma_d = \sigma_{\text{time}} \cdot c$, and c stands for speed of light in air. This method can be used for localization quality assessment if the system parameters are known (receiver noise, jitter, and time measurement resolution). More details on the calculation procedure can be found in [16].

4. UWB Hardware and TDoA Setup

4.1. UWB Demonstrator. The UWB demonstrator, built for and used in this experiment, consists of an impulse radio UWB (IR-UWB) transmitter (Tx) and an autocorrelation-based receiver (ACR). The generic transmitter module, presented in Figure 3, consists mainly of a custom pulse generation- (PG-) integrated circuit (IC) and an of-the-shelf amplifier. The PG can be directly fed with digital data, and each time a falling signal slope is present at its input, a UWB pulse is generated. For this architecture, the achievable data rates span from several kbps up to the lower Gbps region.

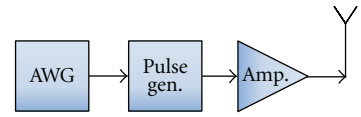

Figure 3: Block diagram of the IR-UWB transmitter module.

The hardware realization of the described transmitter is presented in Figure 4. In the picture, the following elements are visible (starting from the left side): UWB pulse generator [17], amplifier together with a bias tee, variable attenuator, and an omnidirectional antenna (planar monopole).

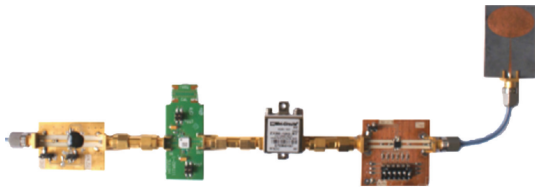

Figure 4: UWB transmit module realized in hardware.

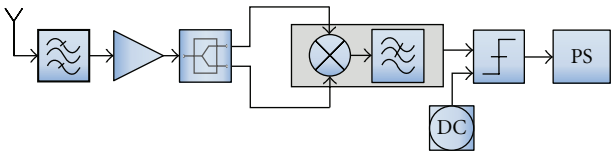

Figure 5: Block diagram of the energy detection receiver.

The variable attenuator module (not present in Figure 3) is used to flexibly adjust the amplitude of the transmitted signal, depending on the pulse repetition frequency, to match the FCC spectral emission mask [5].

The UWB receiver (Rx) is presented in Figure 5. After the receive antenna, the signal is band-pass filtered and amplified. Although the arrangement of the filter and the LNA influences the receiver noise figure in a bad manner, out-of-band interference has to be filtered out first to avoid the saturation of the following amplifier. Afterwards, the signal is equally divided and squared. The low-pass-filtered multiplier output is compared with DC threshold, generating a digital signal. The last block is responsible for the signal conditioning.

In Figure 6, the hardware realization of the ACR is illustrated. Starting from the left, the following components are depicted: the directive receive antenna (Vivaldi type), 7th-order microstrip FCC band-pass filter, wideband LNA [18], 3 dB power splitter, UWB correlator module (with an integrated base band amplifier) [19], variable threshold comparator, and the pulse stretcher.

The last module ensures that the receiver output signal (rectangular pulse) has always the same width and amplitude. This is essential for proper operation of the time-to-digital converter (see next section). More information about the performance of the transceiver single building blocks can be found in [20, 21].

4.2. TDC and TDoA Measurement Setup. For the precise time measurements, a time-to-digital converter (TDC) has been used. This device is used to measure the time elapsed between appearance of two (or more) signals at its input ports. First incoming signal generates a *start* and the following ones, the *stop* events. The device of choice for this experiment is the TDC produced by Acam, model ATMD-GPX. This model, depending on the operating mode, is capable of detecting two incoming digital signals with up to 27 ps resolution. A maximum of up to eight input ports can be used.

In Figure 7, a typical system setup for TDoA measurement is shown. The APs are interconnected to ensure

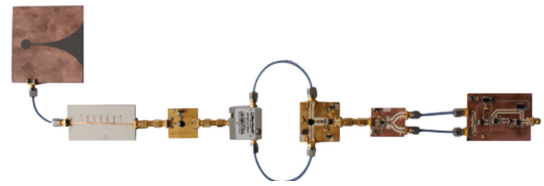

Figure 6: Hardware realization of a UWB autocorrelation receiver.

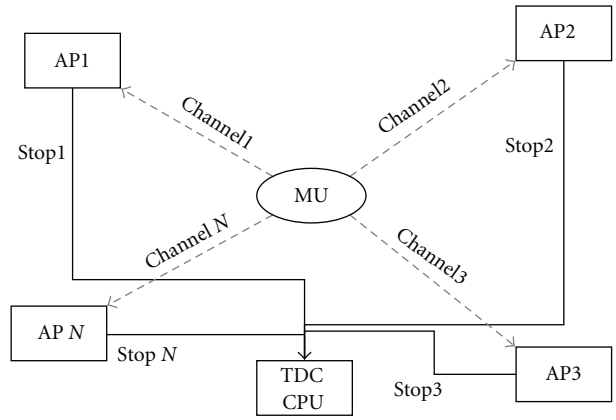

Figure 7: Typical TDoA localization system architecture. Synchronized APs receive UWB signals from an autonomous MU, which then are used to calculate its position.

synchronization and an autonomic MU equipped with an UWB tag transmits the impulses. The signals propagate through the scenario on physically different paths (channels) and reach the AP. The received signals from all APs are forwarded to the time measurement unit (TDC) through the synchronization network. The received signals undergo certain delays ($T_{\text{stop}\,N}$) before they trigger the time measurement at TDC. This can be described with

$$T_{\text{meas}\,N} = T_{\text{channel}\,N} + T_{\text{Rx}} + T_{\text{stop}\,N} + T_{\text{offset}}, \quad (22)$$

where the T_{Rx} stands for the AP-specific delay. T_{offset} originates from the fact that the MU is not synchronized with the APs, and the transmission time point is unknown. The first received impulse triggers the TDC measurement, and the differences to the following impulses are calculated. Such a system requires an initial calibration to determine the T_{Rx} and $T_{\text{stop}\,N}$. After substituting the $T_{\text{meas}\,N}$ into the TDoA equations, the T_{offset} is eliminated.

Due to the limited number of the UWB receivers available for this experiment, the measurements were conducted with one Tx and one Rx unit in a sequential manner. The time measurement procedure for the single MU-AP pair is demonstrated in Figure 8.

In this setup, the (22) is modified and the resulting measured time can be described by following relation:

$$T_{\text{meas}\,N} = T_{\text{trig}} + T_{\text{Tx}} + T_{\text{channel}\,N} + T_{\text{Rx}} + T_{\text{stop}} - T_{\text{start}}, \quad (23)$$

where the variables have the following meaning: T_{trig} is the delay caused by the triggering cable, T_{Tx} is the time between the trigger enters the Tx and the moment when

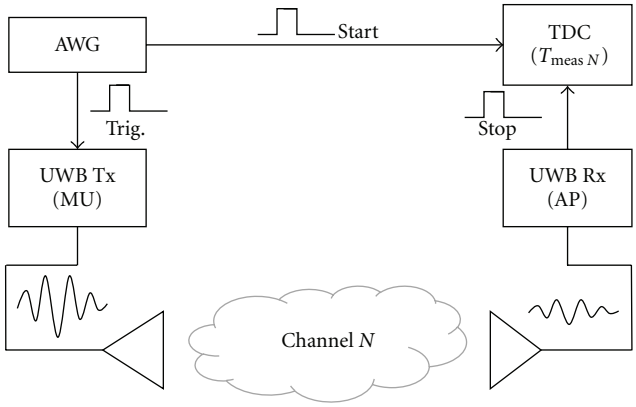

Figure 8: Setup for measuring the signal propagation time between MU and AP with the TDC module.

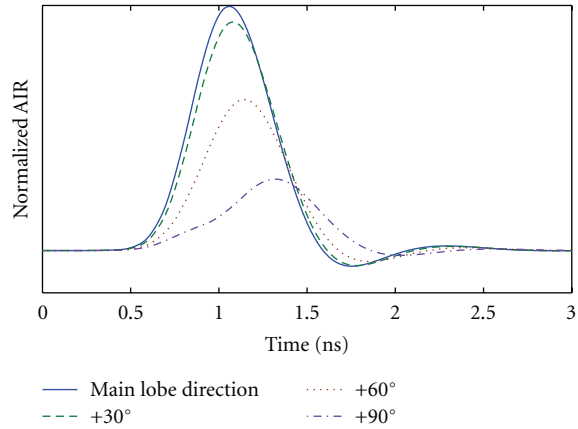

Figure 9: Simulation of the angle-dependent impulse response of the applied AP antenna.

the UWB pulse reaches the transmit antenna, $T_{\text{channel}\,N}$ is the propagation time through the Nth channel, T_{Rx} is the time required by the Rx to process the signal and convert it to digital domain, T_{stop} is the propagation time through a cable to the TDC unit, and finally, the T_{start} is the time after the signal reaches the TDC. In case where the same system components were used for measurements at each AP ($N = 1$ to 5), all the terms in (23), with exception of $T_{\text{channel}\,N}$, are constant. After building the time differences with $T_{\text{meas }N}$ according to (1), a true TDoA data set is obtained.

5. Sources of Timing Errors

In this section, the sources of inaccurate signal time of arrival measurements will be discussed. They can either originate from passive RF devices in the system or from active digital electronics. The two most critical time error contributions are discussed below.

5.1. Antenna Influence. In the recent years, a significant number of antennas were proposed for different UWB applications. The antenna is one of the most crucial devices in any wireless system. It is responsible for matching the 50 Ohm system impedance (most common) to the free-space impedance. In the ideal case, this would happen without any losses and distortion of the transmitted signal. In practice however, this is never the case. As reported in [22], the influence of the antennas in the UWB transmission cannot be neglected. The different types of broadband radiating devices introduce signal distortions, which in most cases are additionally angle dependent [23]. The parameter that describes the time domain characteristic is the antenna impulse response (AIR). The shape of the AIR and the delay of its maximum can cause an additional offset during the TDoA measurements. According to this, the localization accuracy of the MU will be additionally dependent on the relative angle under which the AP antenna is oriented with respect to the MU.

In the application scenario, described in Section 6, there is no initial information about the MU position. This implies that the signals should be sent/received to/from all directions with equal probability. To reach all APs, the MU antenna should exhibit an omnidirectional radiation pattern. On the other hand, the AP antennas will preferably have a certain directive pattern, to illuminate only a certain part of the scenario.

In the conducted experiment, the mobile user is equipped with an omnidirectional antenna (planar *monopole*), having a uniform characteristic in the horizontal plane (equal pulse distortion). Due to the time difference approach, the influence of the MU antenna can be neglected, because the distortions are the same in each direction. For the AP, antennas with a directive radiation characteristic (*Vivaldi* type) were used. In Figure 9, the distortion of the AP AIR in dependency on angle is visualized. It can be observed that the time shift of the AIRs maximum, during the change of angle (horizontal plane) from the main radiation direction to the perpendicular position, equals 260 ps.

After analyzing the scenario depicted Figures 13 and 14, AP antennas can be oriented in a way that the 90° reception angle would not be needed. However, an additional time delay of up to 200 ps could be introduced, when operated in an angular range of ±60°. This value corresponds to the distance of 6 cm in the free space. From this, it is obvious that this offset can greatly influence the accuracy of the overall system, aiming for lower subdecimeter accuracy. The method to eliminate the influence of the used antenna is based on an iterative approach and should be presented in the following. The only requirement for this algorithm is the knowledge about spatial orientation of the AP antennas. This can easily be assured during the system deployment phase. The flow chart of this algorithm is depicted in Figure 10.

After obtaining a valid TDoA measurement, the first step is the standard calculation of the positioning solution. This will lead to a first solution, which will serve as a starting point for the iteration. Knowing the approximate MU location, the relative angles between APs reference direction and estimated MU position can be calculated. For those angles, the time correction factors for each AP can be obtained from the lookup table (LUT). The LUT contains the information about the delay of the AIRs peak, relative to the reference direction (e.g., main lobe direction), for all angles.

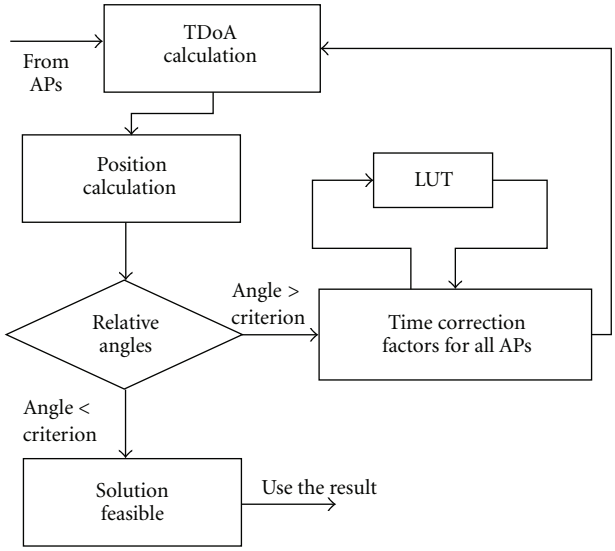

Figure 10: Schematic representation of the AIR influence correction algorithm.

After subtracting the correction factors from the original time differences, the new position can be calculated. This operation can be reperformed until a break criterion is met, for example, if the change in the relative angle between two iterations is smaller than a certain value. Other type of criterion would be the change in the calculated positioning solution. The resulting position can now be further used for applications like, for example, tracking.

5.2. Threshold Detection. In every system, there is an interface between analog and digital domain. At this place, both amplitude and time errors can appear. Depending on the digitizing device (comparator or ADC with more than one-bit resolution), the amplitude error will have different values. Obviously, the ADCs with 8 bits, or even more, are capable of transforming the signal into digital domain with only marginal amplitude distortion. The problem with high-resolution ADCs nowadays is their limited bandwidth. Therefore, and because of their cost and power consumption (e.g., pipe-line ADCs consume over 1 W), they will rather not find application in UWB systems for the mass market. Comparators are less accurate, but by far cheaper and seem to be a much better alternative for this application. These devices can achieve bandwidths close to 10 GHz and equivalent input signal rise times of 80 ps [24]. The problem that has to be addressed is the choice of the threshold level. In a scenario with large dynamic range, the trigger time dependency on signal level will play an important role. This is depicted in Figure 11. The use of an adaptive threshold would be the optimal solution; however, this is hardly realizable in practice [25].

The influence of the threshold level in a certain scenario can be mitigated in a similar way as in the case of the AIR. After calculating the initial positioning solution for the MU, the time corrections have to be made. Knowing the exact AP coordinates and the estimated coordinates of the MU,

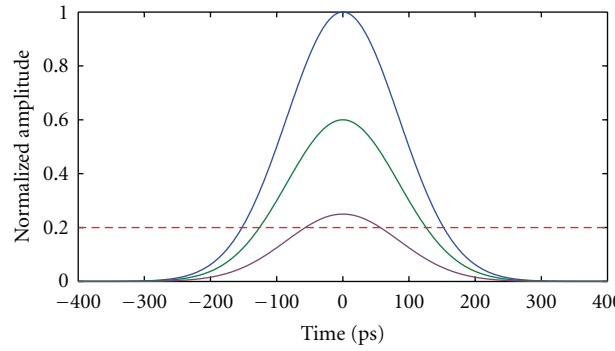

Figure 11: Random walk error-trigger time dependency on threshold level.

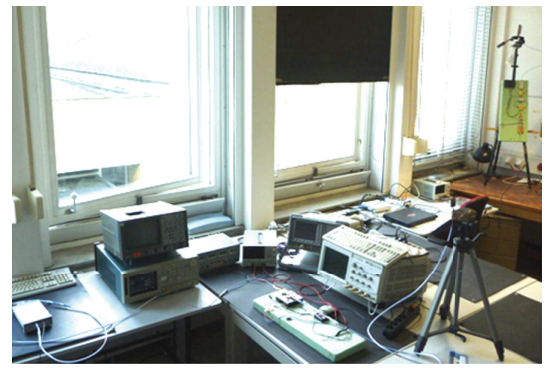

Figure 12: Measurement scenario in a laboratory room. An MU antenna placed on the tripod and the AP antenna in the background (top right).

the differences in distances between all AP-MU pairs can be extracted. Distances correspond to signal attenuation (e.g., based on free space path loss), and this is connected with the received signal amplitude. In the LUT, the estimated relative time trigger errors are saved, which are distance difference dependent. The rest of the correction procedure is the same as in Section 5.1.

The trigger time uncertainty of the comparator, caused by electronic jitter, can be modeled as a stochastic process with normal distribution. The influence of this can be minimized by performing averaging [24]. For similar distances, for example, if the MU is placed near to the center of the AP constellation, this effect is negligible. The reason for this is the TDoA procedure, which cancels all common time offsets.

6. Measurement Scenario and Result Analysis

For the measurement verification of the TDoA-based UWB localization system, the laboratory room at the IHE institute was chosen. The size of the room (W/D/H) is 6.3 m/5.9 m/3 m, and all objects, like furniture and lab equipment, were inside during the measurement, representing an average indoor scenario. The photograph of the scenario is shown in Figure 12.

In this environment, two experiments were conducted. The goal of the *experiment 1* (E1) was to determine

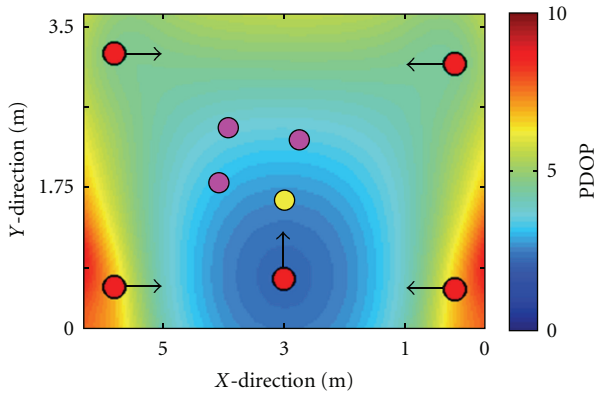

Figure 13: Distribution of the PDOP values (top view) in the simulation and measurement scenario. Red dots represent the AP positions. The yellow dot represents the position of the MU from E1, and magenta those from E2. The arrows show the alignment of the antennas in the E2.

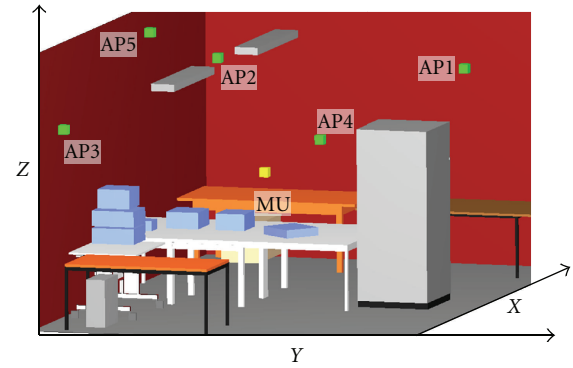

Figure 14: Wave propagation (ray tracer) model of the laboratory room, where the measurements were performed. The green points represent the APs, and the yellow one shows the position of the MU during E1.

Table 2: Positions of the *T*-*R* units in the scenario in E1.

Unit	x [m]	y [m]	z [m]
AP1	5.955	3.030	2.185
AP2	5.955	0.245	2.202
AP3	0.345	0.265	2.165
AP4	0.345	3.152	2.160
AP5	3.145	0.370	2.860
MU	2.985	1.700	1.400

Table 3: Predicted and calculated accuracy for scenarios in E1.

Scenario	Prediction	Accuracy
RT simulation	5.1 ps·3 ⇒ 0.45 cm	0.35 cm
Meas—no avg.	127 ps·3 ⇒ 11.4 cm	11.8 cm
Meas—avg. 50	32 ps·3 ⇒ 2.9 cm	3.6 cm

the achievable positioning accuracy in this environment, comparing the results with the simulation and to validate the method of accuracy prediction. The *experiment 2* (E2) was set up to investigate the influence of the proposed correction algorithms on the positioning accuracy.

6.1. Experiment 1. For validation of the accuracy prediction method, presented earlier in the paper, the system consisting of one MU and five APs was deployed. The positions of the units are listed in Table 2. The same positions were used for the measurement and for simulation.

Based on the positions of the APs, the distribution of the DOP values in the room was calculated. This is presented in Figure 13.

Knowing the method of accuracy prediction (21), a simulation is conducted, to serve as a benchmark for the later measurements. For this purpose, a 3D digital model of the scenario was created, including all the information about objects and their material parameters. In the scenario, the five APs and one MU were placed, at the positions listed in Table 2. Both the scenario model and the deployed devices are shown in Figure 14. The UWB transmission between all Tx-Rx pairs was investigated by means of a three-dimensional wave propagation simulation based on geometric optics (a high-frequency approximation), which uses material parameters (permeability, permittivity, and surface roughness) (RT: ray tracing) [26]. The simulations provide channel impulse responses (CIRs) and are used to obtain the TDoA data.

The time discretization used during the RT simulation results in the CIR peak time determination inaccuracy σ_{time} of 5.1 ps. Multiplying this value with the calculated PDOP, an inaccuracy of 15 ps (corresponding to 4.5 mm distance) is predicted. The calculated solution exhibits an error of 3.5 mm, which lies close to the predicted limit.

In the performed measurement, the receive antennas were all pointing towards the MU. In the horizontal direction, a small alignment variation of ±5° was possible. This fact can lead to an additional positioning error, due to the described AIR angle dependency. The true position of the MU has been determined based on the relative distance measurements to all surrounding walls. This was performed with a laser-based distance measurement device with accuracy of 1 mm.

In the described setup, two data sets have been acquired:

(i) 1023 unaveraged time measurements at each of the five APs. The measurement exhibited a standard deviation (σ_1) of 127 ps. This originates partially from the TDC performance and from the receivers' comparator;

(ii) 1023 time measurements with 50 times averaging at each of the five APs. The standard deviation σ_2 of 32 ps is much closer to the specified performance of the TDC.

In Table 3, the summary of all simulations and measurements, performed up to this moment, is shown. The positioning error prediction is based on (21). The third column shows the mean calculated accuracy.

Table 4: Positions of the mobile units in E2.

Unit	x [m]	y [m]	z [m]
MU1	2.945	2.335	1.2
MU2	3.71	2.435	1.2
MU3	3.885	1.82	1.2

Table 5: Accuracy for no correction and AIR correction.

Unit	Direct TDoA data [m]	100 avg. [m]	100 avg. no outliers [m]	AIR correction [m]
MU1	0.0988	0.0642	0.0327	0.0284
MU2	0.0966	0.0700	0.066	0.0334
MU3	0.0735	0.0343	0.025	0.0135
Average	0.0896	0.0561	0.0412	0.0251

The significant improvement between scenarios 2 and 3 can be explained by the highly reduced comparator trigger error thanks to averaging of the acquired measurements. The reason why during the measurements the errors are slightly larger than predicted is the use of 1σ- and not 3σ-limit. In Figure 15, the calculated MU positions, for the case with averaged time acquisition, are shown. The inaccuracy, resulting from the mean of those solutions, is 3.6 cm.

Overall, this test shows the usefulness of the proposed method of predicting the positioning accuracy, based on PDOP and time acquisition quality.

6.2. Experiment 2. In the second experiment, the effectiveness of the AIR correction method shall be investigated. For this, the same positions of the APs as in the E1 were used. The MU was placed at three different positions in the room to observe the combined influence of antennas and the DOP distribution. The coordinates are listed in Table 4 and depicted in Figure 13. In the same figure, the spatial orientation of the AP antennas can be observed.

In Table 5, the positioning results for all three MUs are shown. In the second column, the solution for direct TDoA data evaluation is shown. In the third column, the positioning result is shown, where the 100-time averaged TDoA measurements were used for localization. In the fourth column, the outliers were removed: from the set of estimated positions the standard dev. was calculated and all values larger than 1σ were not considered. The last column shows the results with performed correction of the antenna influence.

Those results show the effectiveness of the proposed method. The average positioning accuracy improvement, without and with use of the antenna delay compensation method, is 36%. Obviously, the MU1-MU3 were localized with different accuracy; however, this originates solely from the distribution of the DOP values.

7. Summary and Conclusion

In this work, a complete UWB indoor localization demonstrator, dedicated for operation with a predeployed access point infrastructure, has been presented. Different TDoA solution algorithms were implemented and evaluated. The combination consisting of modified Bancroft and Levenberg-Marquardt algorithms was identified as the most efficient one in terms of average computation time and accuracy. Following this, a method of the access point distribution and constellation quality assessment was proposed. Furthermore, a method for positioning accuracy prediction based on time measurement information was derived. The later was then verified based on simulation and experimental measurements in realistic indoor scenario. Additionally, the unwanted influence of the antenna and other system components was described, and algorithms for their mitigation were proposed. This has also been verified by measurement. By applying the methods presented in this paper, the original average accuracy of 9 cm was improved to a value of 2.5 cm. The proposed methods can be universally applied, and their implementation method assures an optimal localization performance, with low-to-moderate computational effort, what is of major importance for future real-time locating systems.

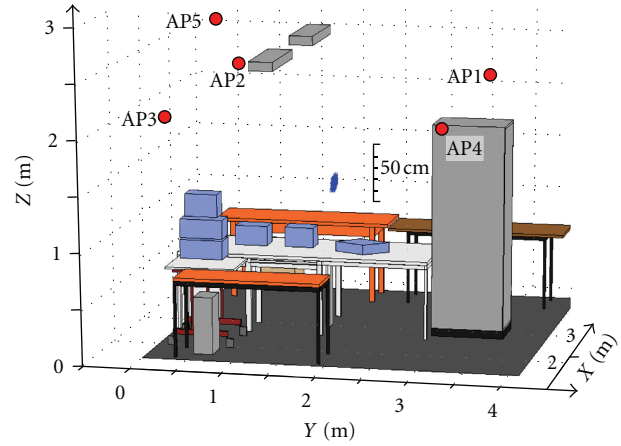

Figure 15: The localization solutions (cloud of blue points in the middle) are plotted into the scenario. The TDoA data comes from the measurements.

Acknowledgments

The authors would like to thank the Baden-Württemberg Stiftung for financing the work, under the research program "Werkzeuge für die flexible, adaptive Produktion 2007–2011, FKZ: Pro09" and the Institute of Electron Devices and Circuits at the University of Ulm for providing the prototypes of the UWB integrated circuits.

References

[1] A. Ward, A. Jones, and A. Hopper, "A new location technique for the active office," *IEEE Personal Communications*, vol. 4, no. 5, pp. 42–47, 1997.

[2] AT&T Laboratories Cambridge, "Active Bat ultrasonic location system," http://www.cl.cam.ac.uk/research/dtg/attarchive/bat/.

[3] S. Hann, J. H. Kim, S. Y. Jung, and C. S. Park, "White LED ceiling lights positioning systems for optical wireless indoor applications," in *36th European Conference and Exhibition on Optical Communication (ECOC '10)*, September 2010.

[4] H. Liu, H. Darabi, P. Banerjee, and J. Liu, "Survey of wireless indoor positioning techniques and systems," *IEEE Transactions on Systems, Man and Cybernetics C*, vol. 37, no. 6, pp. 1067–1080, 2007.

[5] Federal Communications Commission (FCC), "Revision of Part 15 of the Commissions Rules Regarding Ultra Wideband Transmission Systems," First Report and Order, ET Docket 98-153, FCC 02-48; Adopted: February 2002; Released: April 2002.

[6] Electronic Communications Committee (ECC), "The harmonised conditions for devices using Ultra-Wideband (UWB) technology in bands below 10.6 GHz," Decision (06)04, Approved: March 2006.

[7] Z. Xiao, G. Tan, R. Li, and K. Yi, "A joint localization scheme based on IR-UWB for sensor network," in *7th International Conference on Wireless Communications, Networking and Mobile Computing (WiCOM '11)*, September 2011.

[8] G. Fischer, O. Klymenko, D. Martynenko, and H. Luediger, "An impulse radio UWB transceiver with high-precision TOA measurement unit," in *International Conference on Indoor Positioning and Indoor Navigation (IPIN '10)*, Zurich, Switzerland, September 2010.

[9] A. De Angelis, M. Dionigi, A. Moschitta, R. Giglietti, and P. Carbone, "Characterization and modeling of an experimental UWB pulse-based distance measurement system," *IEEE Transactions on Instrumentation and Measurement*, vol. 58, no. 5, pp. 1479–1486, 2009.

[10] R. Moenikes, *Verwendung differentieller GNSS-Trägerphasenmessungen zur integrierten hochgenauen Positionierung*, Dissertation, Universität Karlsruhe, Institut für theoretische Elektrotechnik (ITE), 2008.

[11] L. Zwirello, M. Janson, and T. Zwick, "Ultra-wideband based positioning system for applications in industrial environments," in *3rd European Wireless Technology Conference (EuWiT '10)*, pp. 165–168, Paris, France, September 2010.

[12] C. Mensing and S. Plass, "Positioning algorithms for cellular networks using TDoA," in *IEEE International Conference on Acoustics, Speech and Signal Processing (ICASSP '06)*, pp. 513–516, Toulouse, France, May 2006.

[13] I. Sharp, K. Yu, and Y. J. Guo, "GDOP analysis for positioning system design," *IEEE Transactions on Vehicular Technology*, vol. 58, no. 7, pp. 3371–3382, 2009.

[14] J. D. Bard and F. M. Ham, "Time difference of arrival dilution of precision and applications," *IEEE Transactions on Signal Processing*, vol. 47, no. 2, pp. 521–523, 1999.

[15] R. B. Langley, "Dilution of Precision," GPS World, May 1999, http://gauss.gge.unb.ca/papers.pdf/gpsworld.may99.pdf.

[16] H. Sairo, D. Akopian, and J. Takala, "Weighted dilution of precision as quality measure in satellite positioning," *IEE Proceedings: Radar, Sonar and Navigation*, vol. 150, no. 6, pp. 430–436, 2003.

[17] B. Schleicher, J. Dederer, M. Leib et al., "Highly compact impulse UWB transmitter for high-resolution movement detection," in *IEEE International Conference on Ultra-Wideband (ICUWB '08)*, pp. 89–92, September 2008.

[18] J. Dederer, S. Chartier, T. Feger, U. Spitzberg, A. Trasser, and H. Schumacher, "Highly compact 3.1–10.6 GHz UWB LNA in SiGe HBT technology," in *10th European Conference on Wireless Technology (ECWT '07)*, pp. 327–330, October 2007.

[19] J. Dederer, B. Schleicher, A. Trasser, T. Feger, and H. Schumacher, "A fully monolithic 3.1–10.6 GHz UWB Si/SiGe HBT Impulse-UWB correlation receiver," in *IEEE International Conference on Ultra-Wideband (ICUWB '08)*, pp. 33–36, September 2008.

[20] L. Zwirello, Ch. Heine, X. Li, and T. Zwick, "An UWB correlation receiver for performance assessment of synchronization algorithms," in *IEEE International Conference on Ultra-Wideband (ICUWB '11)*, Bologna, Italy, September 2011.

[21] L. Zwirello, P. Pahl, Ch. Heine, and T. Zwick, "Status Report on the FCC-Compliant UWB Transceiver Implementation," in *6th UWB Forum on Sensing and Communication*, Graz, Austria, May 2011.

[22] W. Wiesbeck, G. Adamiuk, and C. Sturm, "Basic properties and design principles of UWB antennas," *Proceedings of the IEEE*, vol. 97, no. 2, pp. 372–385, 2009.

[23] E. Pancera, T. Zwick, and W. Wiesbeck, "Spherical fidelity patterns of UWB antennas," *IEEE Transactions on Antennas and Propagation*, vol. 59, no. 6, pp. 2111–2119, 2011.

[24] J. Kolakowski, "Application of ultra-fast comparator for UWB pulse time of arrival measurement," in *IEEE International Conference on Ultra-Wideband (ICUWB '11)*, September 2011.

[25] R. J. Fontana, "Ultra wideband receiver with high speed noise and interference tracking threshold," US Patent 005901172, 1999.

[26] T. Fugen, J. Maurer, T. Kayser, and W. Wiesbeck, "Capability of 3-D ray tracing for defining parameter sets for the specification of future mobile communications systems," *IEEE Transactions on Antennas and Propagation*, vol. 54, no. 11, pp. 3125–3137, 2006.